Escherichia coli NusG links the lead ribosome with the transcription elongation complex

Robert S. Washburn[1], Philipp K. Zuber[2], Ming Sun[3,4], Yaser Hashem[5,6], Bingxin Shen[5,7], Wen Li[5], Sho Harvey[8,9], Stefan H. Knauer[2,*], Joachim Frank[3,5,*], and Max E. Gottesman[1,5,*]

[1]Department of Microbiology & Immunology, Columbia University Medical Center, New York, NY 10032, USA.

[2]Biopolymers, University of Bayreuth, Universitaetsstrasse 30, 95447 Bayreuth, Germany.

[3]Department of Biological Sciences, Columbia University, New York, NY 10027, USA.

[4]Current address: University of California at San Francisco, San Francisco, CA 94158, USA.

[5]Department of Biochemistry and Molecular Biophysics, Columbia University Medical Center, New York, NY 10032, USA.

[6]Current address: NSERM U1212, Institut Européen de Chimie et Biologie, University of Bordeaux, Pessac 33607, France.

[7]Current address: Bristol-Myers Squibb Pharmaceutical Co., New Brunswick, NJ 08901, USA.

[8]University of Michigan, Ann Arbor, MI 48109, USA.

[9]Current address: California Institute of Technology, Pasadena, CA 91125, USA.

*Corresponding Authors

Abstract

It has been known for more than 50 years that transcription and translation are physically coupled in bacteria, but whether or not this coupling may be mediated by the two-domain protein N-utilization substance (Nus) G in *Escherichia coli* is still heavily debated. Here, we combine integrative structural biology and functional analyses to provide conclusive evidence that NusG can physically link transcription with translation by contacting both RNA polymerase and the ribosome. We present a cryo-electron microscopy structure of a NusG:70S ribosome complex and nuclear magnetic resonance spectroscopy data revealing simultaneous binding of NusG to RNAP and the intact 70S ribosome, providing the first direct structural evidence for NusG-mediated coupling. Furthermore, *in vivo* reporter assays show that recruitment of NusG occurs late in transcription and strongly depends on translation. Thus, our data suggest that coupling occurs initially via direct RNAP:ribosome contacts and is then mediated by NusG.

Introduction

Gene expression is a universal process in all cells and consists of transcription, i.e. the synthesis of RNA based on the DNA, and – if RNA is not the final gene product – translation, i.e. the messenger RNA (mRNA)-guided synthesis of a protein. Since the late 1960s it has been known that the rates of transcription and translation are synchronized in *Echerichia coli* so that mRNA is translated while being transcribed (Das et al., 1967; Mehdi and Yudkin, 1967; Miller et al., 1970; Proshkin et al., 2010; Vogel and Jensen, 1995, 1994). This process,called transcription:translation coupling, is possible due to the lack of a physical barrier between transcription and translation in bacteria (reviewed in (Conn et al., 2019)). Only recently, direct physical interactions between RNA polymerase (RNAP) and the ribosomes have been demonstrated (Demo et al., 2017; Fan et al., 2017; Kohler et al., 2017), consistent with earlier observations that transcriptional events may control translation activity and *vice versa*(Proshkin et al., 2010). As transcription and translation are closely connected to other central processes in a bacterial cell, such as DNA repair (Pani and Nudler, 2017) and protein folding (Thommen et al., 2017), transcription:translation coupling constitutes one of the key resulatory functions in bacterial gene expression.

However, there are also indications that transcription:translation coupling may involve a member of the family of N-utilization substance (Nus) G proteins, which serves as adapter connecting RNAP and the lead ribosome (Burmann et al., 2012, 2010; Saxena et al., 2018; Zuber et al., 2019). *E. coli* Nus G, member and eponym of the only universally conserved class of transcription factors (Werner, 2012), consists of two

62 domain, an N- and a C-terminal domain (NTD and CTD, resepectively) connected v*ia* a
63 flexible linker, which move independently (Burmann et al., 2011; Mooney et al., 2009).
64 NusG-NTD binds RNAP and accelerates transcription elongation (Burova et al., 1995;
65 Kang et al., 2018; Mooney et al., 2009). Structural studies demonstrate that NusG-CTD,
66 which is a five-stranded β-barrel with a Kyrpides-Ouzounis-Woese motif (Kyrpides et al.,
67 1996), is a versatile binding platform for different transcription factors. By binding to
68 protein S10, which is part of the 30S subunit of the ribosome, NusG may link
69 transcription and translation (Burmann et al., 2010). Saxena *et al* also demonstrated
70 specific 1:1 binding of NusG to 70S ribosomes both *in vitro* and *in vivo* (Saxena et al.,
71 2018).

72 S10 is identical with transcription factor NusE and forms a ribosome-free
73 complex with NusB, NusA and NusG which suppresses transcription termination
74 (Dudenhoeffer et al., 2019; Krupp et al., 2019; Said et al., 2017; Squires et al., 1993).
75 Finally, NusG-CTD binds to termination factor Rho and is required for most Rho activity
76 *in vivo* (Burmann et al., 2010; Lawson et al., 2018; Mitra et al., 2017).
77 Transcription:translation coupling prevents Rho factor from terminating transcription by
78 sequestering the NusG-CTD and by blocking Rho access to RNAP via untranslated
79 mRNA. Cryptic *E. coli* Rho-dependent terminators located within open reading frames
80 (orfs) are revealed when ribosomes are released by polar nonsense mutations (Cardinale
81 et al., 2008; Newton et al., 1965).

82 Nevertheless, there is evidence for intragenic uncoupling and Rho-dependent
83 transcription termination in the absence of nonsense mutations. Washburn and
84 Gottesman (Washburn and Gottesman, 2011) and Dutta et al. (Dutta et al., 2011) found

that Rho resolves clashes between transcription and replication. Such conflicts are likely to occur within, rather than at the end of, genes. Uncoupling would allow Rho to release the stationary transcription elongation complexes (TECs).

Mutations in *nusE* or *nusG* that uncouple transcription from translation increase sensitivity to chloramphenicol (Saxena et al., 2018). This antibiotic retards translation, breaking the bond between the lead ribosome and TEC. Uncoupled TEC may backtrack or terminate prematurely (Dutta et al., 2011).

In this report, we present a cryo-electron microscopy (cryo-EM) structure showing NusG binding to the S10 subunit in a 70S ribosome. The NusG-CTD binding site of S10 is also target of the ribosome-release factor, transfer-messenger (tmRNA), raising the possibility that tmRNA might displace NusG at rare codons, thereby uncoupling transcription from translation (Roche and Sauer, 1999). We also show by solution-state nuclear magnetic resonance (NMR) spectroscopy that NusG, once bound to RNAP, can interact with S10 or with a complete ribosome, setting the structural basis for coupling.

NusG couples transcription with translation *in vivo*, as proposed earlier (Burmann et al., 2010). Uncoupling of RNAP from the lead ribosome is enhanced when translation is compromised. Importantly, we demonstrate that uncoupled RNAP can outpace translation, leading to Rho-dependent transcription termination. This intragenic termination explains the necessity for the apparent perfect synchronization between transcription and translation (Proshkin et al., 2010).

Results

Structural evidence of NusG binding to the ribosomal S10 subunit on a 70S ribosome.

We assembled a NusG:70S complex by incubating 70S ribosomes with an excess of NusG and determined the structure of this complex by cryo-EM and single-particle reconstruction. Overall, 188,127 particles were extracted from 1327 images and ~5% of these particles showed an extra mass of density attached to the mass identified as protein S10 (Fig. 1A,B). This additional density perfectly matches the size of NusG-CTD, suggesting that NusG binds at the site predicted from the solution NMR structure of NusG-CTD bound to the free ribosomal protein S10 in a 1:1 stoichiometry (Fig. 1A,B; (Burmann et al., 2010)). The density map reconstructed from the class of NusG:70S particles was refined to an average resolution of 6.8 Å. No density could be observed for NusG-NTD, indicating that it is flexibly bound to the NusG-CTD and does not interact with the ribosome.

During translation ribosomes may stall on incomplete mRNAs, i.e. they reach the 3' end of an mRNA without terminating, resulting in an unproductive translation complex. Together with the small protein B (SmpB) tmRNA can bind to these stalled ribosomes in order to rescue them and to tag the nascent polypeptide chain for degradation in a process called trans-translation (Weis et al., 2010). Interestingly, the NusG-CTD binding site overlaps with the region of S10 that is contacted by the tmRNA when it is bound to a ribosome in its resume state (Fig. 1C; (Burmann et al., 2010; Fu et al., 2010; Rae et al., 2019; Weis et al., 2010)). From this we conclude that NusG-CTD and tmRNA share binding sites on S10, raising the possibility that, in addition to

130 releasing stalled ribosomes, tmRNA competes with NusG for ribosome binding, thus
131 preventing NusG from maintaining a linkage between the lead ribosome and RNAP. In
132 other words, tmRNA might be able to displace NusG and thereby facilitate uncoupled
133 transcription.
134
135 **Simultaneous binding of NusG to S10 and RNAP**
136 In the cryo-EM structure of *E. coli* NusG bound to a paused TEC (Kang et al., 2018) only
137 the density of NusG-NTD was observable, indicating that NusG-CTD moves freely and
138 does not interact with RNAP. Binding of NusG-CTD to S10 was observed both in a
139 binary system (Burmann et al., 2010) and a λN-dependent antitermination complex
140 (Krupp et al., 2019; Said et al., 2017).
141 Since the NusG-CTD:S10 interaction is a prerequisite for NusG-mediated
142 transcription:translation coupling, we probed this contact when NusG was bound to
143 RNAP - but not in an antitermination context - by solution-state NMR spectroscopy. We
144 employed NusG samples where [^{1}H,^{13}C]-labeled methyl groups of Ile, Leu, and Val
145 residues in perdeuterated proteins served as NMR-active probes ([ILV]-NusG) to
146 increase sensitivity, allowing us to study large systems.
147 In the methyl-transverse relaxation optimized spectroscopy (methyl-TROSY)
148 spectrum of free [ILV]-NusG (Fig. 2A), signals of the NusG-NTD and NusG-CTD
149 perfectly superimpose with the signals of the isolated [ILV]-labeled protein domains,
150 suggesting that the domains move independently, confirming a previous report stating
151 that there are no intramolecular domain interactions (Burmann et al., 2011). Upon
152 addition of RNAP in a two-fold molar excess, [ILV]-NusG signals were significantly

153 decreased in the one-dimensional methyl-TROSY spectrum (Fig. 2B, inset), indicating
154 [ILV]-NusG:RNAP complex formation. Binding of RNAP increases the molecular mass
155 of [ILV]-NusG dramatically, resulting in enhanced relaxation, which ultimately leads to
156 drastic line broadening and a decrease in signal intensity. Interestingly, the two-
157 dimensional spectra revealed a non-uniform signal decrease (Fig. 2B), which is caused by
158 a combination of several effects. First, there is a general loss of signal intensity due to the
159 increase in molecular mass upon complex formation, as discussed above. Second, upon
160 binding, methyl groups of Ile, Leu, and Val residues located in the binding surface come
161 into close proximity of RNAP protons. Dipole-dipole interactions contribute to relaxation
162 processes so that the signal intensity of these methyl groups is decreased more strongly
163 than that of methyl groups located elsewhere in [ILV]-NusG. Finally, signal intensities
164 may be affected by chemical exchange processes. We analyzed the signal intensity of
165 [ILV]-NusG signals in the presence of RNAP quantitatively by calculating relative signal
166 intensities, i.e. the ratio of the remaining signal intensity of [ILV]-NusG in the presence
167 of RNAP to the signal intensity of free [ILV]-NusG (Figure 2-figure supplement 1).

168 The average relative intensity of NusG-NTD signals was significantly lower than
169 that of the linker or the NusG-CTD, suggesting that NusG-NTD binds to RNAP whereas
170 NusG-CTD remains flexible and moves independently, able to interact with other
171 partners, as indicated by the NusG:TEC structure (Kang et al., 2018). The signal intensity
172 of all Ile, Leu, and Val residues in the RNAP binding site of NusG was completely
173 extinguished, confirming that NusG-NTD binds to RNAP at its known binding site
174 (Drögemüller et al., 2015; Kang et al., 2018; Krupp et al., 2019; Said et al., 2017).

To test if NusG-CTD can bind to S10 while being tethered to RNAP *via* NusG-NTD, we titrated the [ILV]-NusG:RNAP complex with $S10^{\Delta}$ (Fig. 2C). In order to increase stability, we used this S10 variant lacking the ribosome binding loop in complex with NusB (Luo et al., 2008). Chemical shift changes of [ILV]-NusG-CTD signals upon titration of [ILV]-NusG:RNAP with $S10^{\Delta}$:NusB were determined (Fig. 2D) and affected residues were mapped onto the three-dimensional structure of NusG-CTD (Fig. 2E). Strongly affected residues are found to be located in β-strands 3 and 4 as well as in the connecting loop, in agreement with the binding site observed in the binary NusG-CTD:$S10^{\Delta}$ complex (Burmann et al., 2010). The loop between β-strands 1 and 2 is also part of the NusG-CTD:$S10^{\Delta}$ binding site, but as it does not contain any Ile, Leu, or Val residues, no NMR-active probes are available in this region; nevertheless, affected residues can be found in β-strand 1, directly preceding this loop. This suggests that the CTD:$S10^{\Delta}$ binding surface in the RNAP:NusG:$S10^{\Delta}$:NusB complex is identical to the one determined in the binary system. Importantly, the NusG-NTD signals do not change when S10 is added to the NusG:RNAP complex, indicating that S10 binding does not release the bound RNAP.

We conclude that the S10 interaction site of NusG-CTD is accessible in the NusG:RNAP complex and thus can promote ribosome binding and formation of a ribosome:NusG:RNAP complex.

To look for a ribosome:NusG-RNAP complex, we repeated the experiment using intact 70S ribosomes instead of $S10^{\Delta}$:NusB (Figure 3). In a first test, we titrated [ILV]-NusG with 70S ribosomes (Figure 3A). As in the [ILV]-NusG:RNAP experiment, signal

intensity of [ILV]-NusG methyl groups was significantly, but not uniformly, decreased. In the presence of a twofold molar excess of ribosomes some NusG-NTD signals remained visible, whereas most NusG-CTD signals were nearly completely extinguished. Quantitative analysis of the [ILV]-NusG methyl group signal intensity in the presence of 0.5 equivalents of 70S ribosomes clearly shows that the relative intensity of NusG-CTD signals was in a narrow range < 2 %, whereas the relative intensity of NusG-NTD signals covered values from 0-4 %, and was higher on average (Figure 3B). Relative intensities of zero of NusG-NTD signals can be attributed to the fact that these signals are weak even in free NusG, and can thus not be quantified upon ribosome binding. Due to the flexibility of the linker, signals corresponding to amino acids in this region had the highest relative signal intensities. From these results we conclude that NusG binds to the ribosome via its CTD, in agreement with our cryo-EM structure (Figure 1). Due to the drastic increase in molecular mass we were unable to determine a binding site from these experiments, but nevertheless, the pattern of intensity changes of NusG-CTD signals was similar to that resulting form the titration of RNAP-bound NusG with S10, i.e. the most drastic decrease of signal intensity can be observed for residues 160-170, which are part of β-strands 3 and 4 and the intervening loop. Consequently, we conclude that the ribosome binding site is identical with the binding site for isolated S10.

Next, we formed a complex of [ILV]-NusG and RNAP (molar ratio 1:2). The 2D methyl-TROSY spectrum of the complex revealed a decrease of signal intensities typical for NusG binding to RNAP (see Fig. 2C), i.e. primarily NusG-CTD signals remained visible. When we then added one equivalent of 70S ribosomes nearly all [ILV]-NusG signals were diminished (e.g. the signal corresponding to I164, which is in the loop

221 responsible for ribosome binding). Strikingly, the spectrum differs from the spectrum of
222 [ILV]-NusG in the presence of 70S ribosome (Fig. 3A). These results can be explained
223 by three scenarios: (i) NusG-NTD is bound to RNAP, NusG-CTD is bound to a
224 ribosome, and the ribosome directly interacts with RNAP, (ii) NusG-NTD is bound to
225 RNAP, NusG-CTD is bound to the ribosome, but the ribosome does not interact with
226 RNAP, (iii) NusG-NTD is bound to RNAP, the ribosome directly interacts with RNAP,
227 and NusG-CTD is free, but is in the vicinity of the ribosome. To exclude the last scenario
228 we repeated the experiment using a NusG variant, NusG^{F165A}, in which F165, essential
229 for ribosome binding (Burmann et al., 2010; Knowlton et al., 2003), is substituted by an
230 Ala. Having ensured that the amino acid substitution does not influence the structure of
231 NusG (Fig. 3-figure supplement 1A) we tested in a control experiment [ILV]-NusG^{F165A}
232 binding to S10^{A}. Indeed, we could detect no interaction (Fig. 3-figure supplement 1B,C).
233 When we added 70S ribosomes to a preformed [ILV]-NusG^{F165A}:RNAP complex (molar
234 ratio 2:1), the spectrum corresponding to the [ILV]-NusG^{F165A}:RNAP complex did not
235 significantly change and, in particular, NusG-CTD signals remained visible, suggesting
236 that the ribosome was not bound. However the general decrease in signal intensity
237 indicated a direct RNAP:ribosome interaction. Thus, we conclude that NusG can serve as
238 physical linker between ribosome and RNAP, although it remains elusive if a direct
239 interaction between RNAP and a ribosome occurs in this NusG-coupled complex.
240
241 **Translation promotes NusG attachment to TEC.**
242 Chromatin Immuno Precipitation (ChIP) analysis showed that NusG binds to TEC well
243 after transcription and translation initiation (Mooney et al., 2009). Thus, we asked

whether translation was, in fact, required for attachment of NusG to TEC. To approach this question, we examined the effects of translation on NusG-mediated Rho-dependent termination within the *lac* operon (Fig. 4A, Table 1) as NusG recruitment to the TEC is necessary for efficient Rho-dependent termination. Rho-dependent termination occurs within *lacZ* both *in vitro* (Burns and Richardson, 1995) and, upon the introduction of *lacZ* nonsense mutations, *in vivo* (Adhya and Gottesman, 1978; Newton et al., 1965). Polarity was measured using a probe to *lacA*, comparing mRNA levels with or without treatment with the Rho inhibitor bicyclomycin (BCM). Wildtype (WT) cells revealed no detectable termination (Table 1, Fig. 4A-I), which may be attributed to (i) sequestering of NusG-CTD by the ribosome, (ii) binding of the ribosome to the nascent RNA, or (iii) both. In all scenarios, however, the presence of the translating ribosome prevents Rho binding. We interfered with translation initiation by mutating the ribosome-binding site, i.e. the Shine-Dalgarno (SD) sequence (Fig. 4A-II), or translation elongation by introducing six successive rare arginine codons at two different locations in *lacZ* (Fig. 4A III, IV). Introduction of two G to A mutations in the *lacZ* SD sequence prohibits translation initiation of *lacZ* (Fig. 4A-II). *lacA* mRNA measurements gave a read-through of 21%, indicating that Rho-dependent termination occurs, but was inefficient in the absence of translation of *lacZ* mRNA. Introduction of the six in-frame rare arginine residues at the +4 position of *lacZ* (Fig. 4A-III, Table 1) allowed 29% read-through, i.e. Rho-dependent termination is present, but still inefficient if translation of *lacZ* mRNA is interfered with at early elongation. In contrast, introduction of the rare arginine residues 200 nt from the start site of transcription (Fig. 4A-IV, Table 1) resulted in high polarity, yielding < 1 %

266 read-through. As efficient Rho-dependent termination requires NusG our results suggests
267 that NusG binding to TEC occurs late and is dependent on translation.

268 To confirm the hypothesis that NusG failed to attach to TEC in the absence of
269 translation, we asked if a complex comprising Nus factors A, B, and E (Nus complex)
270 assembled at a λ *nutL* site was able to recruit NusG so that it associates with TEC.
271 Accordingly, we introduced the λ *nutL* site just upstream of the flawed *lacZ* SD sequence
272 and measured *lacA* mRNA (Figure 4B, Table 1). Indeed, Rho-dependent termination was
273 highly efficient, indicating that NusG had been recruited to TEC. Thus,
274 counterintuitively, the Nus complex, which normally suppresses transcription termination
275 in ribosomal (*rrn*) operons and, together with λN, on the phage λ chromosome,
276 stimulates termination in this case.

277 We finally demonstrated that reduced termination efficiency in the mutant with
278 the non-functional SD sequence was due to the failure of NusG recruitment to the TEC.
279 In this assay we monitored Rho-dependent termination in a fusion construct that carries
280 λ *cro,* the λ *nutR* site, the Rho-dependent λ *tR1* terminator and a *lacZ* reporter, with *lacZ*
281 expression being heat-inducible (Fig. 5). Termination at the λ *tR1* site is poor when *cro* is
282 translated, as seen with the *cro ms27* fusion (Table 2A, Fig. 5A-I; in the presence of an
283 intact SD sequence we used *cro ms27*, where codon 27 carries a missense mutation so
284 that the resulting protein is non-functional). The 3' end of *cro* is adjacent to the λ *tR1*
285 terminator, limiting the amount of free RNA available for Rho attachment if *cro* mRNA
286 is translated. When λ *cro* carried a SD mutation translation initiation was ablated, but
287 nevertheless there was significant termination at λ *tR1* (Table 2A, Figure 5A-II, compare
288 read-through values with and without BCM). Formation of the Nus complex at λ *nutR*

289 allows NusG recruitment and efficient termination. In the absence of NusB, the complex
290 does not assemble, and there is extensive read-through at λ *tR1*.

291 The *boxA69* mutation also reduces Nus complex formation at λ *nutR*, and like the
292 *nusB*- mutation, enhances read-through of λ *tR1* (Table 2B, Fig. 5B). In this experiment,
293 we suppressed termination at λ *tR1* with λ N antitermination factor instead of BCM.
294 Finally, we showed that expression of *nusG-NTD*, which competes with NusG for
295 binding to RNAP, enhances read-through (Table 2C, Fig. 5C). Taken together, these
296 results strongly support the idea that NusG can be supplied by the Nus complex
297 assembled at λ *nutR* in the absence of translation, inducing Rho-dependent termination at
298 λ *tR1*.
299

Discussion

We determined a cryo-EM structure of a NusG: 70S complex showing binding of one molecule NusG per ribosome, consistent with previous results (Saxena et al., 2018). NusG binds to the S10 protein on the 30S subunit via its CTD as indicated by the study of isolated NusG-CTD and S10 (Burmann et al., 2010); density for NusG-NTD was not observable, suggesting that it remains flexible. We must attribute the low occupancy of the NusG CTD on the 70S ribosome in the cryo-EM experiment to weak binding adversely affected by the conditions of sample preparation. Notably, although tmRNA contacts the ribosome at various sites, the binding of NusG-CTD and tmRNA on S10 is mutually exclusive. This suggests a model in which uncoupling at rare codons, at which tmRNA releases ribosomes, is promoted by tmRNA-induced release of NusG (Roche and Sauer, 1999). The freed NusG:TEC complex exposes the NusG-CTD, and is then subject to Rho-dependent transcription termination.

Simultaneous binding of NusG to S10 and RNAP has been demonstrated by solution-state NMR studies, confirming the S10 binding site on NusG-CTD as identified in a binary NusG-CTD:S10 system (Fig. 2) (Burmann et al., 2010). Moreover, we show that NusG can bind RNAP and 70S ribosome simultaneously; this is the first direct structural evidence for NusG-mediated transcription:translation coupling. The flexibility of the linker between the NusG-NTD and the NusG-CTD permits these interactions. The operon-specific *E. coli* NusG paralog, RfaH, likewise simultaneously binds S10 and RNAP in the context of a paused TEC (Burmann et al., 2012; Zuber et al., 2019). RfaH, which also comprises an NTD and a flexibly-connected CTD (Belogurov et al., 2007; Burmann et al., 2012), uses the same binding sites as NusG to interact with RNAP and

S10 (Burmann et al., 2012, 2010; Kang et al., 2018; Sevostyanova et al., 2011; Zuber et al., 2019). However, RfaH, unlike NusG, complexes with TEC early after transcription initiation, when TEC pauses at an operon polarity suppressor (*ops*) site, a representative of the *E. coli* consensus pause sequence (Larson et al., 2014; Vvedenskaya et al., 2014). Located in the untranslated leader region of RfaH-controlled operons, *ops* is responsible for sequence-specific recruitment of RfaH (Zuber et al., 2018). Importantly, RfaH-dependent operons lack a SD sequence. To initiate translation, RfaH recruits a ribosome to these mRNAs, making coupling essential for translation activation and efficient gene expression. The binding modes of RfaH and NusG to RNAP and S10 are very similar, indicating that coupling as observed for RfaH can also be mediated by NusG and vice versa. However, once recruited, RfaH excludes NusG, thus preventing intra-operon Rho-dependent transcription termination in RfaH-controlled operons (see (Artsimovitch and Knauer, 2019)).

We have confirmed the results of Mooney et al that NusG binds to TEC only after significant RNA synthesis (Mooney et al., 2009). As postulated by these authors, binding depends on active translation of the mRNA. Thus efficient Rho-dependent transcription termination, which requires the attachment of Rho to the NusG-CTD, does not occur at the end of an untranslated gene. We have shown that the failure of NusG to bind TEC is responsible for the absence of termination. Thus, placing a λ *nut* site at the start of the gene recruits NusG and restores termination. At present, it is not understood why NusG appears to be delivered to TEC by ribosomes *in vivo*, whereas it binds directly to RNAP in a purified system lacking ribosomes. A possible explanation would be that NusG binds to RNAP discontinuously in an on-and-off mode in the untranslated leader region and

346 that the NusG:RNAP interaction is only stabilized when the ribosome is coupled upon
347 translation initiation. We should recall that NusG has two binding sites in the coupled
348 system, which significantly increases its affinity.

349 In 1970, Miller *et al.* performed electron miscroscopy analyses of lysed *E. coli*
350 cells (Miller et al., 1970). They demonstrated that all mRNA molecules are connected to
351 the *E. coli* genome, and that the ribosome at the newly synthesized end of a polyribosome
352 is almost always immediately adjacent to the putative RNAP molecule. They concluded
353 that translation is completely coupled with transcription. Since NusG attaches to the TEC
354 downstream to the translation initiation site, the elongating complex must initially consist
355 of a ribosome bound directly to TEC, in agreement with the cryo-EM structures of an
356 expressome (Kohler et al., 2017) and an RNAP:30S complex (Demo et al., 2017), as well
357 as *in vitro* data (Fan et al., 2017). At some distance downstream, NusG recognizes and
358 enters the complex. A cryo-EM analysis of a ribosome:RNAP complex reveals a structure
359 with sufficient flexibility to accept NusG between the ribosome and RNAP (Demo et al.,
360 2017). These authors suggest that NusG could enter the complex late, in agreement with
361 our data. Thus we hypothesize that two coupling modes exist, a direct coupling between
362 the ribosome and TEC during translation initiation and early elongation and a NusG-
363 mediated coupling mode later in translation. The question of whether the 70S ribosome
364 still directly contacts TEC in the NusG-mediated system remains elusive. The Kohler
365 structure (Kohler et al., 2017) does not allow NusG binding to TEC and the 70S
366 ribosome, thus the relative orientation of 70S ribosome to TEC might be different in the
367 direct and the NusG-mediated system. The latter may thus require a reorientation of the
368 TEC and the 70S ribosome and confer the system more flexibility, necessary to keep

369 transcription and translation synchronized, even if these processes are differently
370 regulated or occur at different rates.
371

Methods

Strain Construction. Standard bacteriological techniques used in strain construction (e.g., transformation, transduction and media preparation) are as described in Silhavy et al. (Silhavy et al., 1984). Standard molecular biology techniques were as described in Sambrook and Russell (Sambrook and Russel, 2001). N10780 was constructed by P1 transduction of *rpoC-his:kanR nusGF165A* from NB885 into MDS42. N11158 was constructed by P1 transduction of Δ*ssrA::camR* from RSW943 into MDS42. N11816 was constructed by P1 transduction of Δ*relA::kanR* from RLG847 into N11158. RSW1008 was constructed by P1 transduction of Δ*ssrA::camR* from RSW943 into N4837. RSW1010 was constructed by P1 transduction of *rpoC-his:kanR nusGF165A* from NB885 into N4837. RSW1012 was constructed by P1 transduction of Δ*ssrA::camR* from RSW943 into RSW1010. RSW1175 was constructed by P1 transduction of *ΔrelA::kanR* and *ΔspoT::camR* from RLG847 into MDS42. RSW1245 was generated using recombineering (Sharan et al., 2009) to introduce six rare arginine codons (atg-acc-atg-AGG-AGA-CGA-AGG-AGA-CGA-att-acg-gat) into the 5'end of *lacZ* in MDS42 changing the amino acid sequence of the aminoterminus from MTMITD to MTMRRRRRRITD with six inefficiently translated arginine codons. RSW1225 was produced using recombineering to introduce two G to A mutations in the ribosome binding site of *lacZ* in MDS42. This resulted in a change from …TTCACACAGGAAACAGCTatgaccatg… to …TTCACACACC AAACAGCTatgaccatg…inactivating the ribosome binding site. RSW1225 is *lac*$^-$.

394

395 **Cloning.** The plasmid encoding NusG-F165A was generated by site-directed
396 mutagenesis according to the QuikChange Site-Directed Mutagenesis Kit (Stratagene),
397 using vector pET11A_*nusG* (Burmann et al., 2011) as template and primers Fw_NusG-
398 F165A (5' GTG TCT GTT TCT ATC GCG GGT CGT GCG ACC CCG 3') and
399 Rv_NusG-F165A (5' CGG GGT CGC ACG ACC CGC GAT AGA AAC AGA CAC 3';
400 both primers were obtained from metabion, Martinsried, Germany).

401

402 **Protein production and isotopic labeling.** NusG and NusG-NTD were produced as
403 described (Burmann et al., 2011) as were NusG-CTD (Burmann et al., 2010) and RNAP
404 and $S10^{\lambda}$:NusB used for NMR spectroscopy (Zuber et al., 2019). Production of NusG-
405 F165A was analogous to NusG (Burmann et al., 2011). For unlabeled proteins, bacteria
406 were grown in lysogeny broth (LB) medium. [^{1}H,^{13}C]-labeling of methyl groups of Ile,
407 Leu, and Val residues in perdeuterated proteins was accomplished by growing bacteria in
408 M9 medium (Meyer and Schlegel, 1983; Sambrook and Russel, 2001) prepared with
409 increasing amounts of D_2O (0 % (v/v), 50 % (v/v), 100 % (v/v); Eurisotop, Saint-Aubin,
410 France) and $(^{15}NH_4)_2SO_4$ (CortecNet, Voisins-Le-Bretonneux, France) and d_7-glucose
411 (Cambridge Isotope Laboratories, Inc., Tewksburgy, USA) as sole nitrogen and carbon
412 sources, respectively. Amino acid precursors (60 mg/l 2-keto-3-d_3-4-^{13}C-butyrate and 100
413 mg/l 2-keto-3-methyl-d_3-3-d_1-4-^{13}C-butyrate; Eurisotop, Saint-Aubin, France) were
414 added 1 h prior to induction. Expression and purification protocols were identical to those
415 of the non-labeled proteins.

Intact 70S ribosomes were produced as follows. *E. coli* strain MRE600 cells grown in LB medium were harvested, lysed by passing through the French Press 3x at ~800 PSI, and clarified by a short centrifugation (20,000 rpm, 40min) in opening buffer (20 mM Tris-HCl pH=7.5, 100mM NH_4Cl, 10.5 mM Mg acetate, 0.5 mM EDTA, with half a protease inhibitor cocktail tablet (Roche, EDTA-free), and 1mM TCEP added just before use). The lysate was loaded onto the top of 5 mL sucrose cushion (20 mM Tris-HCl, pH=7.5, 500 mM NH_4Cl, 10.5 mM Mg acetate, 0.5 mM EDTA, 1.1 M sucrose, and 1 mM TCEP added before use) and centrifuged for 24 h at 28,000 rpm in a 70Ti rotor (Beckman Coulter, Inc.). The pellets were suspended in washing buffer (20 mM Tris-HCl, pH=7.5; 500mM NH_4Cl, 10.5mM Mg acetate, 0.5mM EDTA and 1 mM TCEP added before use), and centrifuged through a 10–35% sucrose gradient for 19 h at 16,000 rpm in a SW28 rotor (Beckman Coulter, Inc.). Fractions containing the 70S peaks were pooled and kept at -80℃ for further use.

Ribosomes for NMR experiments were obtained from New England Biolabs.

Electron Microscopy

Purified 70S ribosomes were incubated with full-length NusG at a ratio of 1:7 for 40 min at room temperature, prior to blotting and plunge-freezing as previously described (Grassucci et al., 2007). Data were collected on a TF30 Polara electron microscope (FEI, Portland, Oregon) at 300kV using a K2 Summit direct electron detector camera (Gatan, Pleasanton, CA). Images were recorded using the automated data collection system Leginon (Suloway et al., 2005) in counting mode, and taken at the nominal magnification of 32,000x, corresponding to a calibrated pixel size of 1.66Å.

439 **Image processing**

440 A total of 188,127 particles were automatically extracted from 1327 images using
441 Arachnid (Langlois et al., 2014). RELION (Scheres, 2012) 3D classification was used to
442 resolve the heterogeneity of the particle images, and auto-refinement to further improve
443 resolution for each class. The final refinement for the NusG-bound 70S class containing
444 17,122 particles yielded an average resolution of ~6.8Å (FSC=0.143; following "gold
445 standard" protocol).

446

447 **Model building**

448 The starting model was assembled from the X-ray structure of the *E. coli* 30S ribosomal
449 subunit (PDB ID 4GD2) and the NMR solution structure of the NusG-CTD (PDB 2KVQ
450 chain G). This starting model was first docked into the segmented maps of our 70S
451 density map as a rigid body using UCSF Chimera (Pettersen et al., 2004). Then it was
452 fitted into the segmented map using the Molecular Dynamic Flexibly Fitting (MDFF)
453 method (Trabuco et al., 2008) and run using the NAMD program (Phillips et al., 2005) for
454 0.5 ns of simulation time, followed by 5,000 steps of energy minimization.

455

456 **NMR spectroscopy.** NMR experiments were conducted on Bruker Ascend Aeon 900 and
457 1000 MHz spectrometers equipped with cryogenically cooled, inverse triple resonance
458 probes at 298 K. NMR data was converted and processed using in-house software. 2D
459 correlation spectra were visualized and analyzed with NMRViewJ (One Moon Scientific,
460 Inc., Westfield, NJ, USA), 1D spectra were plotted using MatLab (The MathWorks, Inc.,

461 Version 9.2.0.538062). Resonance assignments for NusG methyl groups were taken from
462 a previous study (Mooney et al., 2009).
463 [ILV]-NusG-CTD was in 10 mM K-phosphate (pH 7.5), 50 mM KCl, 1 mM $MgCl_2$, 99.9
464 % (v/v) D_2O, [ILV]-NusG-NTD in 50 mM Na-phosphate (pH 7.5), 50 mM KCl, 0.3 mM
465 EDTA, 5 % (v/v) d_7-glycerol, 0.01 % (w/v) NaN_3, 99.9 % D_2O. For the titration of [ILV]-
466 NusG with RNAP and $S10^D$:NusB, all proteins were in 50 mM Na-phosphate (pH 7.5),
467 50 mM KCl, 0.3 mM EDTA, 99.9 % (v/v) D_2O and 5 mM $MgCl_2$ and 2 mM DTT were
468 added to the NMR sample to increase the-long-term stability of RNAP. For all interaction
469 studies involving ribosomes and for the titration of [ILV]-NusG-F165A with $S10^A$:NusB,
470 all components were in 20 mM HEPES-KOH (pH 7.6), 10 mM Mg-acetate, 30 mM KCl,
471 7 mM β-mercaptoethanol, 10 % D_2O. The titration of [ILV]-NusG-F165A with
472 $S10^A$:NusB was conducted in a 5 mm tube with an initial sample volume of 550 µl. All
473 other measurements were carried out in 3 mm NMR tubes with an (initial) volume of 200
474 µl.
475 1D and 2D titration experiments were evaluated quantitatively by analyzing either
476 changes in signal intensity or changes in chemical shifts. If chemical shift changes were
477 in the fast regime on the chemical shift the normalized chemical shift perturbation
478 ($\Delta\delta_{norm}$) was calculated according to equation 1.
479

480 $$\Delta\delta_{norm} = \sqrt{\left(\Delta\delta\ ^1H\right)^2 + \left[0.25\ \left(\Delta\delta^{13}C\right)\right]^2} \quad (1)$$

481 with Δδ being the resonance frequency difference between the initial and final state of the
482 titration (i.e. [ILV]-NusG:RNAP:$S10^D$:NusB = 1:2:0:0 *vs*. 1:2:2:2) in ppm.
483

If the system was in slow or intermediate chemical exchange the signal intensities were analyzed quantitatively. First, the intensity of each 1D spectrum or methyl group signal, respectively, was normalized by the concentration of the [ILV]-labeled protein, the receiver gain, the number of scans, and the length of the 90° ^{1}H pulse. Then the relative intensity, i.e. the ratio of the normalized signal intensity of [ILV]-labeled protein in the respective titration step to the normalized signal intensity of free [ILV]-labeled protein, was calculated and plotted against the sequence of NusG or the NusG variant, respectively.

q**RT-PCR.** Total RNA was extracted from cells grown in M9 medium supplemented with casamino acids (0.2%) at 37^{0}C to mid-log phase (O.D. 600=0.3). Fold-increase of the PCR product was determined using qRT-PCR. cDNA was synthesized using RNA was extracted from logarithmically growing cultures ($O.D._{600}$=0.2-0.3) Where indicated, cells were treated with BCM (100μg/ml) 1 min before induction with 1mM IPTG for *lacZ*. Samples were removed (0.5ml) at the indicated times and total RNA extracted RNA extracted using Qiagen RNeasy and Qiagen RNAprotect Bacteria Reagent (Qiagen, Germantown, MD). cDNA was synthesized from the samples using High Capacity RNA to cDNA kit (ThermoFisher, Waltham, MA). qRT-PCR reactions were performed using Taqman Gene Expression Master Mix (Thermofisher, Waltham, MA) and Biorad DNA Engine Opticon2 Real-Time Cycler (Bio-Rad Laboratories, Hercules, CA) and PrimeTime qPCR probes (Integrated DNA Technologies, Coralville, IA). The *lacA* transcript was probed with the following: probe:5'-/56-FAM/CCACATGAC/ZEN/TTCCGATCCAGACGTT/3IABkFQ/-3'; primer1:5'-

ATACTACCCGCGCCAATAAC; primer2:5'-CCCTGTACACCATGAATTGAGA). The reference gene was *ompA*(probe:5'-/56-FAM/CAACAACAT/ZEN/CGGTGACGCACACAC /3IABkFQ/-3'; primer1:5'-TGACCGAAACGGTAGGAAAC; primer2:5'-ACGCGATCACTCCTGAAATC). The PCR was performed using the following conditions: 50 °C for 10 min., 95 °C for 2 min, followed by 40 cycles each of 95 °C for 15s, and 60 °C 1min. All reactions were performed in duplicate. Fold increases were calculated from measured C_t values using the $\Delta\Delta C_t$ method (Livak and Schmittgen, 2001). Values are the average of three or more independent experiments.

β–galactosidase assays. Cultures were grown in LB to early log phase (O.D. 600 =0.3) at 37 ^{0}C. Where indicated bicyclomycin (BCM) (100μg/ml) was added to inhibit Rho-dependent transcription termination prior to induction of *lacZ* with 1mm IPTG. Where indicated λN was expressed by incubation at 42 °C. Reactions were terminated 15 min. after induction. β-galactosidase was measured using a modification of the method of Miller (Zhang and Bremer, 1995). Readthrough was calculated from the ratio of β-galactosidase activity +/- BCM.

525 **Author Contributions:** R.W., Y.H., M.S., W.L., B.S. P.K.Z. and S.H. performed the
526 experiments. J.F., Y.H., M.S., R.W. P.K.Z. S.H.K. and M.G. designed the experiments
527 and interpreted the results. M.S. M.G. M.S. P.K.Z. S.H.K. and J.F. wrote the paper.
528
529 **Acknowledgments:** We gratefully acknowledge the help of D. Shapoval, M. Bubunenko,
530 N. Costantino and D. Court. We have had numerous useful discussions with P. Roesch
531 and his group, for which we are most indebted. Supported by HHMI and NIH R01
532 GM29169 (to J.F.), NIH R01 GM037219 (to M.G.) and the German Research
533 Foundation grant Ro617/21-1 (to P.R.). S.H. was supported by an Amgen Fellowship.
534
535 **Competing interests.** We declare no competing interests.

References

Adhya S, Gottesman M. 1978. Control of transcription termination. *Annu Rev Biochem* **47**:967–996. doi:10.1146/annurev.bi.47.070178.004535

Artsimovitch I, Knauer SH. 2019. Ancient Transcription Factors in the News. *MBio* **10**. doi:10.1128/mBio.01547-18

Belogurov GA, Vassylyeva MN, Svetlov V, Klyuyev S, Grishin NV, Vassylyev DG, Artsimovitch I. 2007. Structural basis for converting a general transcription factor into an operon-specific virulence regulator. *Mol Cell* **26**:117–129. doi:10.1016/j.molcel.2007.02.021

Burmann BM, Knauer SH, Sevostyanova A, Schweimer K, Mooney RA, Landick R, Artsimovitch I, Rösch P. 2012. An α helix to β barrel domain switch transforms the transcription factor RfaH into a translation factor. *Cell* **150**:291–303. doi:10.1016/j.cell.2012.05.042

Burmann BM, Scheckenhofer U, Schweimer K, Rösch P. 2011. Domain interactions of the transcription-translation coupling factor *Escherichia coli* NusG are intermolecular and transient. *Biochem J* **435**:783–789. doi:10.1042/BJ20101679

Burmann BM, Schweimer K, Luo X, Wahl MC, Stitt BL, Gottesman ME, Rösch P. 2010. A NusE:NusG complex links transcription and translation. *Science* **328**:501–504. doi:10.1126/science.1184953

Burns CM, Richardson JP. 1995. NusG is required to overcome a kinetic limitation to Rho function at an intragenic terminator. *Proc Natl Acad Sci USA* **92**:4738–4742. doi:10.1073/pnas.92.11.4738

Burova E, Hung SC, Sagitov V, Stitt BL, Gottesman ME. 1995. *Escherichia coli* NusG

559 protein stimulates transcription elongation rates in vivo and in vitro. *J Bacteriol*
560 **177**:1388–1392. doi:10.1128/jb.177.5.1388-1392.1995
561 Cardinale CJ, Washburn RS, Tadigotla VR, Brown LM, Gottesman ME, Nudler E. 2008.
562 Termination factor Rho and its cofactors NusA and NusG silence foreign DNA in *E. coli*.
563 *Science* **320**:935–938. doi:10.1126/science.1152763
564 Conn AB, Diggs S, Tam TK, Blaha GM. 2019. Two Old Dogs, One New Trick: A
565 Review of RNA Polymerase and Ribosome Interactions during Transcription-Translation
566 Coupling. *Int J Mol Sci* **20**. doi:10.3390/ijms20102595
567 Das HK, Goldstein A, Lowney LI. 1967. Attachment of ribosomes to nascent messenger
568 RNA in *Escherichia coli*. *J Mol Biol* **24**:231–245. doi:10.1016/0022-2836(67)90329-4
569 Demo G, Rasouly A, Vasilyev N, Svetlov V, Loveland AB, Diaz-Avalos R, Grigorieff N,
570 Nudler E, Korostelev AA. 2017. Structure of RNA polymerase bound to ribosomal 30S
571 subunit. *Elife* **6**. doi:10.7554/eLife.28560
572 Drögemüller J, Strauß M, Schweimer K, Jurk M, Rösch P, Knauer SH. 2015.
573 Determination of RNA polymerase binding surfaces of transcription factors by NMR
574 spectroscopy. *Sci Rep* **5**:16428. doi:10.1038/srep16428
575 Dudenhoeffer BR, Schneider H, Schweimer K, Knauer SH. 2019. SuhB is an integral part
576 of the ribosomal antitermination complex and interacts with NusA. *Nucleic Acids Res*
577 **47**:6504–6518. doi:10.1093/nar/gkz442
578 Dutta D, Shatalin K, Epshtein V, Gottesman ME, Nudler E. 2011. Linking RNA
579 polymerase backtracking to genome instability in *E. coli*. *Cell* **146**:533–543.
580 doi:10.1016/j.cell.2011.07.034
581 Fan H, Conn AB, Williams PB, Diggs S, Hahm J, Gamper HB, Hou Y-M, O'Leary SE,

582 Wang Y, Blaha GM. 2017. Transcription-translation coupling: direct interactions of RNA
583 polymerase with ribosomes and ribosomal subunits. *Nucleic Acids Res* **45**:11043–11055.
584 doi:10.1093/nar/gkx719
585 Fu J, Hashem Y, Wower I, Lei J, Liao HY, Zwieb C, Wower J, Frank J. 2010.
586 Visualizing the transfer-messenger RNA as the ribosome resumes translation. *EMBO J*
587 **29**:3819–3825. doi:10.1038/emboj.2010.255
588 Grassucci RA, Taylor DJ, Frank J. 2007. Preparation of macromolecular complexes for
589 cryo-electron microscopy. *Nat Protoc* **2**:3239–3246. doi:10.1038/nprot.2007.452
590 Kang JY, Mooney RA, Nedialkov Y, Saba J, Mishanina TV, Artsimovitch I, Landick R,
591 Darst SA. 2018. Structural Basis for Transcript Elongation Control by NusG Family
592 Universal Regulators. *Cell* **173**:1650-1662.e14. doi:10.1016/j.cell.2018.05.017
593 Knowlton JR, Bubunenko M, Andrykovitch M, Guo W, Routzahn KM, Waugh DS,
594 Court DL, Ji X. 2003. A spring-loaded state of NusG in its functional cycle is suggested
595 by X-ray crystallography and supported by site-directed mutants. *Biochemistry* **42**:2275–
596 2281. doi:10.1021/bi0272508
597 Kohler R, Mooney RA, Mills DJ, Landick R, Cramer P. 2017. Architecture of a
598 transcribing-translating expressome. *Science* **356**:194–197. doi:10.1126/science.aal3059
599 Krupp F, Said N, Huang Y-H, Loll B, Bürger J, Mielke T, Spahn CMT, Wahl MC. 2019.
600 Structural Basis for the Action of an All-Purpose Transcription Anti-termination Factor.
601 *Mol Cell*. doi:10.1016/j.molcel.2019.01.016
602 Kyrpides NC, Woese CR, Ouzounis CA. 1996. KOW: a novel motif linking a bacterial
603 transcription factor with ribosomal proteins. *Trends Biochem Sci* **21**:425–426.
604 Langlois R, Pallesen J, Ash JT, Nam Ho D, Rubinstein JL, Frank J. 2014. Automated

particle picking for low-contrast macromolecules in cryo-electron microscopy. *J Struct Biol* **186**:1–7. doi:10.1016/j.jsb.2014.03.001

Larson MH, Mooney RA, Peters JM, Windgassen T, Nayak D, Gross CA, Block SM, Greenleaf WJ, Landick R, Weissman JS. 2014. A pause sequence enriched at translation start sites drives transcription dynamics *in vivo*. *Science* **344**:1042–1047. doi:10.1126/science.1251871

Lawson MR, Ma W, Bellecourt MJ, Artsimovitch I, Martin A, Landick R, Schulten K, Berger JM. 2018. Mechanism for the regulated control of transcription by a universal adapter protein. *Mol Cell* **71**:1–12.

Livak KJ, Schmittgen TD. 2001. Analysis of relative gene expression data using real-time quantitative PCR and the 2(-Delta Delta C(T)) Method. *Methods* **25**:402–408. doi:10.1006/meth.2001.1262

Luo X, Hsiao H-H, Bubunenko M, Weber G, Court DL, Gottesman ME, Urlaub H, Wahl MC. 2008. Structural and functional analysis of the *E. coli* NusB-S10 transcription antitermination complex. *Mol Cell* **32**:791–802. doi:10.1016/j.molcel.2008.10.028

Mehdi Q, Yudkin MD. 1967. Coupling of transcription to translation in the induced synthesis of beta-galactosidase. *Biochim Biophys Acta* **149**:288–290. doi:10.1016/0005-2787(67)90710-1

Meyer O, Schlegel HG. 1983. Biology of aerobic carbon monoxide-oxidizing bacteria. *Annu Rev Microbiol* **37**:277–310. doi:10.1146/annurev.mi.37.100183.001425

Miller OL, Hamkalo BA, Thomas CA. 1970. Visualization of bacterial genes in action. *Science* **169**:392–395. doi:10.1126/science.169.3943.392

Mitra P, Ghosh G, Hafeezunnisa M, Sen R. 2017. Rho Protein: Roles and Mechanisms.

628 *Annu Rev Microbiol* **71**:687–709. doi:10.1146/annurev-micro-030117-020432

629 Mooney Rachel A., Davis SE, Peters JM, Rowland JL, Ansari AZ, Landick R. 2009.

630 Regulator trafficking on bacterial transcription units *in vivo*. *Mol Cell* **33**:97–108.

631 doi:10.1016/j.molcel.2008.12.021

632 Mooney Rachel Anne, Schweimer K, Rösch P, Gottesman M, Landick R. 2009. Two

633 structurally independent domains of *E. coli* NusG create regulatory plasticity via distinct

634 interactions with RNA polymerase and regulators. *J Mol Biol* **391**:341–358.

635 doi:10.1016/j.jmb.2009.05.078

636 Newton WA, Beckwith JR, Zipser D, Brenner S. 1965. Nonsense mutants and polarity in

637 the *lac* operon of *Escherichia coli*. *J Mol Biol* **14**:290–296. doi:10.1016/s0022-

638 2836(65)80250-9

639 Pani B, Nudler E. 2017. Mechanistic insights into transcription coupled DNA repair.

640 *DNA Repair (Amst)* **56**:42–50. doi:10.1016/j.dnarep.2017.06.006

641 Pettersen EF, Goddard TD, Huang CC, Couch GS, Greenblatt DM, Meng EC, Ferrin TE.

642 2004. UCSF Chimera--a visualization system for exploratory research and analysis. *J*

643 *Comput Chem* **25**:1605–1612. doi:10.1002/jcc.20084

644 Phillips JC, Braun R, Wang W, Gumbart J, Tajkhorshid E, Villa E, Chipot C, Skeel RD,

645 Kalé L, Schulten K. 2005. Scalable molecular dynamics with NAMD. *J Comput Chem*

646 **26**:1781–1802. doi:10.1002/jcc.20289

647 Proshkin S, Rahmouni AR, Mironov A, Nudler E. 2010. Cooperation between translating

648 ribosomes and RNA polymerase in transcription elongation. *Science* **328**:504–508.

649 doi:10.1126/science.1184939

650 Rae CD, Gordiyenko Y, Ramakrishnan V. 2019. How a circularized tmRNA moves

through the ribosome. *Science* **363**:740–744. doi:10.1126/science.aav9370

Roche ED, Sauer RT. 1999. SsrA-mediated peptide tagging caused by rare codons and tRNA scarcity. *EMBO J* **18**:4579–4589. doi:10.1093/emboj/18.16.4579

Said N, Krupp F, Anedchenko E, Santos KF, Dybkov O, Huang Y-H, Lee C-T, Loll B, Behrmann E, Bürger J, Mielke T, Loerke J, Urlaub H, Spahn CMT, Weber G, Wahl MC. 2017. Structural basis for λN-dependent processive transcription antitermination. *Nat Microbiol* **2**:17062. doi:10.1038/nmicrobiol.2017.62

Sambrook J, Russel DW. 2001. Molecular Cloning: A Laboratory Manual, Third Edition. ed. New York: Cold Spring Harbor Press.

Saxena S, Myka KK, Washburn R, Costantino N, Court DL, Gottesman ME. 2018. *Escherichia coli* transcription factor NusG binds to 70S ribosomes. *Mol Microbiol* **108**:495–504. doi:10.1111/mmi.13953

Scheres SHW. 2012. RELION: implementation of a Bayesian approach to cryo-EM structure determination. *J Struct Biol* **180**:519–530. doi:10.1016/j.jsb.2012.09.006

Sevostyanova A, Belogurov GA, Mooney RA, Landick R, Artsimovitch I. 2011. The β subunit gate loop is required for RNA polymerase modification by RfaH and NusG. *Mol Cell* **43**:253–262. doi:10.1016/j.molcel.2011.05.026

Sharan SK, Thomason LC, Kuznetsov SG, Court DL. 2009. Recombineering: a homologous recombination-based method of genetic engineering. *Nat Protoc* **4**:206–223. doi:10.1038/nprot.2008.227

Silhavy TJ, Berman ML, Enquist LW, editors. 1984. Experiments with Gene Fusions. Cold Spring Harbor (NY): Cold Spring Harbor Laboratory Press.

Squires CL, Greenblatt J, Li J, Condon C, Squires CL. 1993. Ribosomal RNA

674 antitermination in vitro: requirement for Nus factors and one or more unidentified cellular
675 components. *Proc Natl Acad Sci USA* **90**:970–974.
676 Suloway C, Pulokas J, Fellmann D, Cheng A, Guerra F, Quispe J, Stagg S, Potter CS,
677 Carragher B. 2005. Automated molecular microscopy: the new Leginon system. *J Struct*
678 *Biol* **151**:41–60. doi:10.1016/j.jsb.2005.03.010
679 Thommen M, Holtkamp W, Rodnina MV. 2017. Co-translational protein folding:
680 progress and methods. *Curr Opin Struct Biol* **42**:83–89. doi:10.1016/j.sbi.2016.11.020
681 Trabuco LG, Villa E, Mitra K, Frank J, Schulten K. 2008. Flexible fitting of atomic
682 structures into electron microscopy maps using molecular dynamics. *Structure* **16**:673–
683 683. doi:10.1016/j.str.2008.03.005
684 Vogel U, Jensen KF. 1995. Effects of the antiterminator *BoxA* on transcription elongation
685 kinetics and ppGpp inhibition of transcription elongation in *Escherichia col*i. *J Biol Chem*
686 **270**:18335–18340. doi:10.1074/jbc.270.31.18335
687 Vogel U, Jensen KF. 1994. Effects of guanosine 3',5'-bisdiphosphate (ppGpp) on rate of
688 transcription elongation in isoleucine-starved *Escherichia coli*. *J Biol Chem* **269**:16236–
689 16241.
690 Vvedenskaya IO, Vahedian-Movahed H, Bird JG, Knoblauch JG, Goldman SR, Zhang Y,
691 Ebright RH, Nickels BE. 2014. Interactions between RNA polymerase and the "core
692 recognition element" counteract pausing. *Science* **344**:1285–1289.
693 doi:10.1126/science.1253458
694 Washburn RS, Gottesman ME. 2011. Transcription termination maintains chromosome
695 integrity. *Proc Natl Acad Sci USA* **108**:792–797. doi:10.1073/pnas.1009564108
696 Weis F, Bron P, Giudice E, Rolland J-P, Thomas D, Felden B, Gillet R. 2010. tmRNA-

SmpB: a journey to the centre of the bacterial ribosome. *EMBO J* **29**:3810–3818. doi:10.1038/emboj.2010.252

Werner F. 2012. A nexus for gene expression-molecular mechanisms of Spt5 and NusG in the three domains of life. *J Mol Biol* **417**:13–27. doi:10.1016/j.jmb.2012.01.031

Zhang X, Bremer H. 1995. Control of the Escherichia coli rrnB P1 promoter strength by ppGpp. *J Biol Chem* **270**:11181–11189. doi:10.1074/jbc.270.19.11181

Zuber PK, Artsimovitch I, NandyMazumdar M, Liu Z, Nedialkov Y, Schweimer K, Rösch P, Knauer SH. 2018. The universally-conserved transcription factor RfaH is recruited to a hairpin structure of the non-template DNA strand. *Elife* **7**. doi:10.7554/eLife.36349

Zuber PK, Schweimer K, Rösch P, Artsimovitch I, Knauer SH. 2019. Reversible fold-switching controls the functional cycle of the antitermination factor RfaH. *Nat Commun* **10**:702. doi:10.1038/s41467-019-08567-6

713 **Figures**

714

715

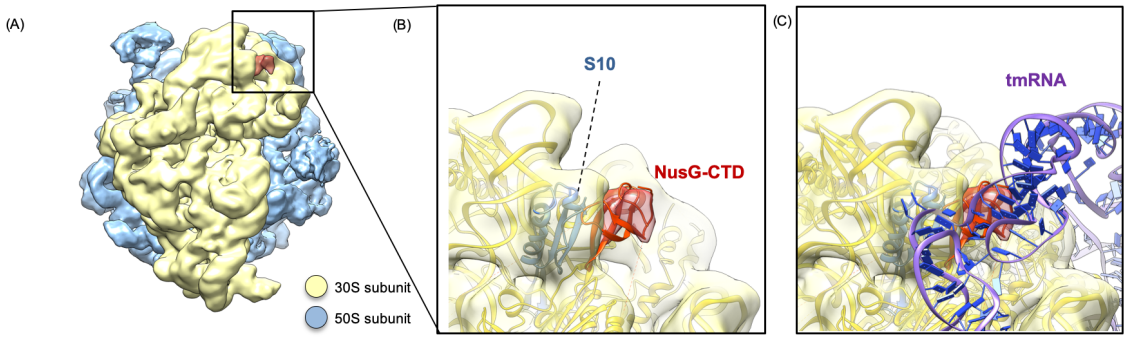

716

717 **Figure 1. Structure of NusG-CTD bound to 70S ribosome. (A)** Cryo-EM density of
718 the 70S ribosome:NusG complex. The density of the 50S subunit is shown in light blue,
719 the density of the 30S subunit in yellow, the density corresponding to NusG-CTD in red.
720 **(B)** Close-up view of the region boxed in **(A)**. 70S (yellow), S10 (blue), and NusG-CTD
721 (red) are in ribbon representation, cryo-EM density is shown as transparencies. **(C)**
722 Superposition of the 70S:NusG complex with the 70S:tmRNA complex (tmRNA is in
723 ribbon representation, purple and dark blue; EMD 5234, PDB: 3IZ4). 30S and NusG-
724 CTD are displayed as in **(B)**.

725

726

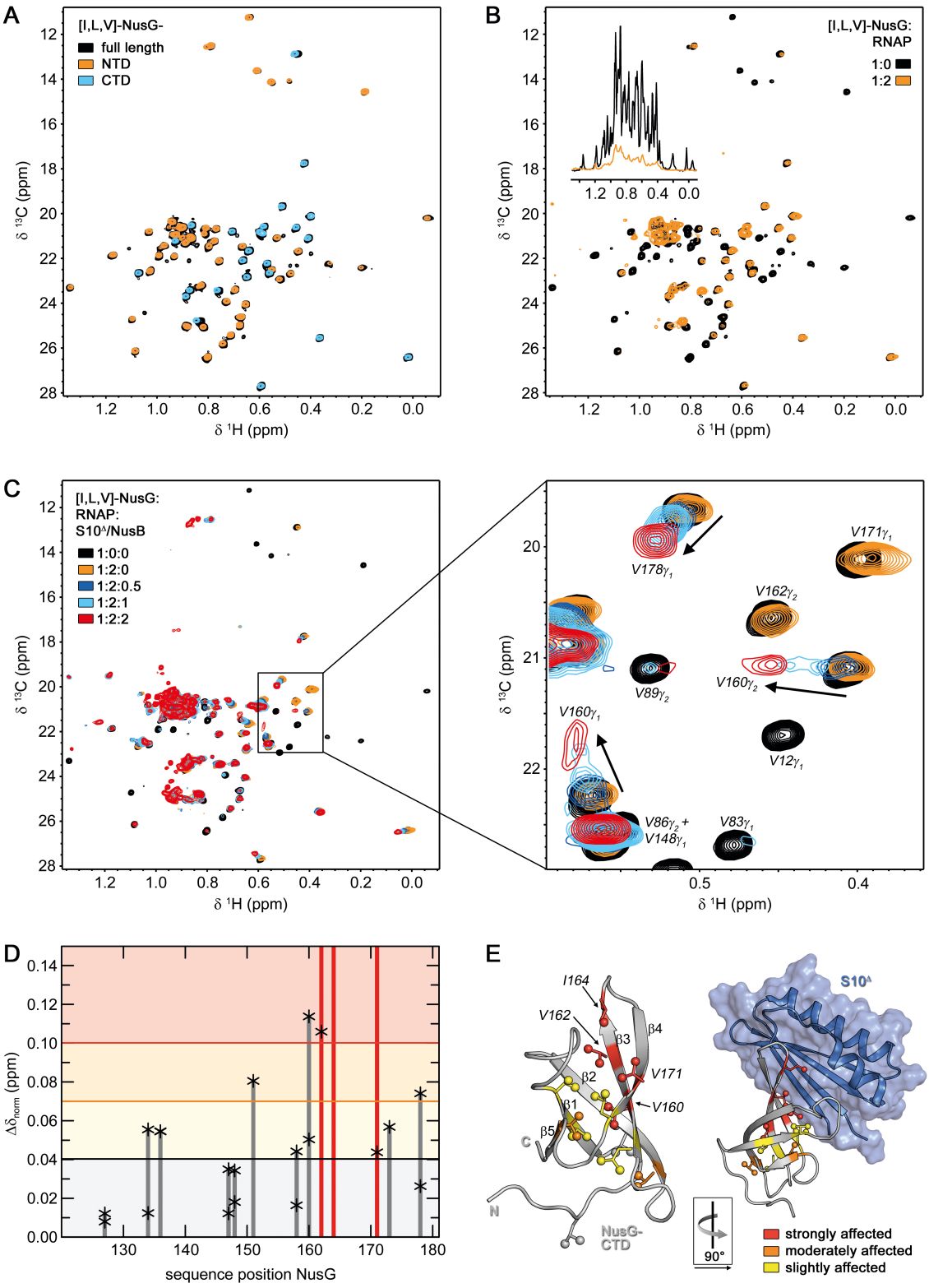

Figure 2. RNAP-bound NusG interacts with S10. (A) Superposition of 2D [^{1}H, ^{13}C]-methyl-TROSY spectra of [ILV]-NusG (black, 20 µM), [ILV]-NusG-NTD (orange, 100

730 μM), and [ILV]-NusG-CTD (cyan, 30 μM). **(B)** 2D [^{1}H, ^{13}C]-methyl-TROSY spectra of
731 [ILV]-NusG in the absence (black, 20 μM) and presence (orange, 18 μM) of two
732 equivalents of RNAP. Inset: Normalized 1D [^{1}H,^{13}C]-methyl TROSY spectra, colored as
733 2D spectra. **(C)** 2D [^{1}H, ^{13}C]-methyl-TROSY spectra of [ILV]-NusG alone (20 μM), in
734 the presence of a twofold molar excess of RNAP (18 μM [ILV]-NusG), and upon
735 titration of [ILV]-NusG:RNAP with 218 μM S10^{A}:NusB. The molar ratio of [ILV]-
736 NusG:RNAP:S10^{A}:NusB is indicated in color. The panel on the right shows an
737 enlargement of the boxed region. Selected signals are labeled and arrows indicate
738 chemical shift changes upon S10^{A}:NusB addition. **(D) [**^{1}H,^{13}C]-methyl-TROSY-derived
739 normalized chemical shift changes of [ILV]-NusG-CTD methyl group signals of RNAP-
740 bound [ILV]-NusG upon complex formation with S10^{A}:NusB. Asterisks mark the values
741 of individual methyl group signals, bars represent the highest values. Red bars indicate
742 vanishing signals. Horizontal lines are thresholds for affected methyl groups: slightly
743 affected (0.04 ppm ≤ $\Delta\delta_{norm}$ < 0.07 ppm; black), moderately affected (0.07 ppm ≤ $\Delta\delta_{norm}$
744 < 0.1 ppm; orange), and strongly affected ($\Delta\delta_{norm}$ ≥ 0.10 ppm; red). **(E)** Mapping of
745 affected methyl groups on the structure of isolated NusG-CTD (left; PDB ID: 2JVV) and
746 NusG-CTD in complex with S10^{A} (right; PDB ID 2KVQ). NusG-CTD is shown in ribbon
747 (gray), S10^{A} in ribbon and surface (blue) representation. Affected Ile, Leu, and Val
748 residues are colored according to **(D),** non-affected Ile, Leu, and Val residues are gray.
749 Side chains of Ile, Leu, and Val residues are depicted as sticks, their methyl groups as
750 spheres. Strongly affected Ile, Leu, and Val residues are labeled. The orientation of
751 NusG-CTD in the complex relative to the isolated state is indicated.
752

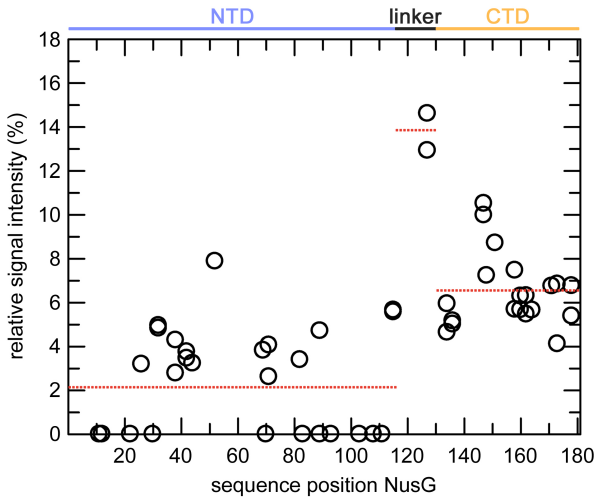

753

754 **Figure 2-figure supplement 1: Binding of [ILV]-NusG to RNAP.** [^{1}H,^{13}C]-methyl-

755 TROSY derived relative signal intensities of [ILV]-NusG methyl groups after addition of

756 two equivalents of RNAP (see Fig. 2B). Red, dashed horizontal lines indicate average

757 relative signal intensities of NusG-NTD, the linker, and NusG-CTD (domain organization

758 is indicated at the top). Related to Figure 2B.

759

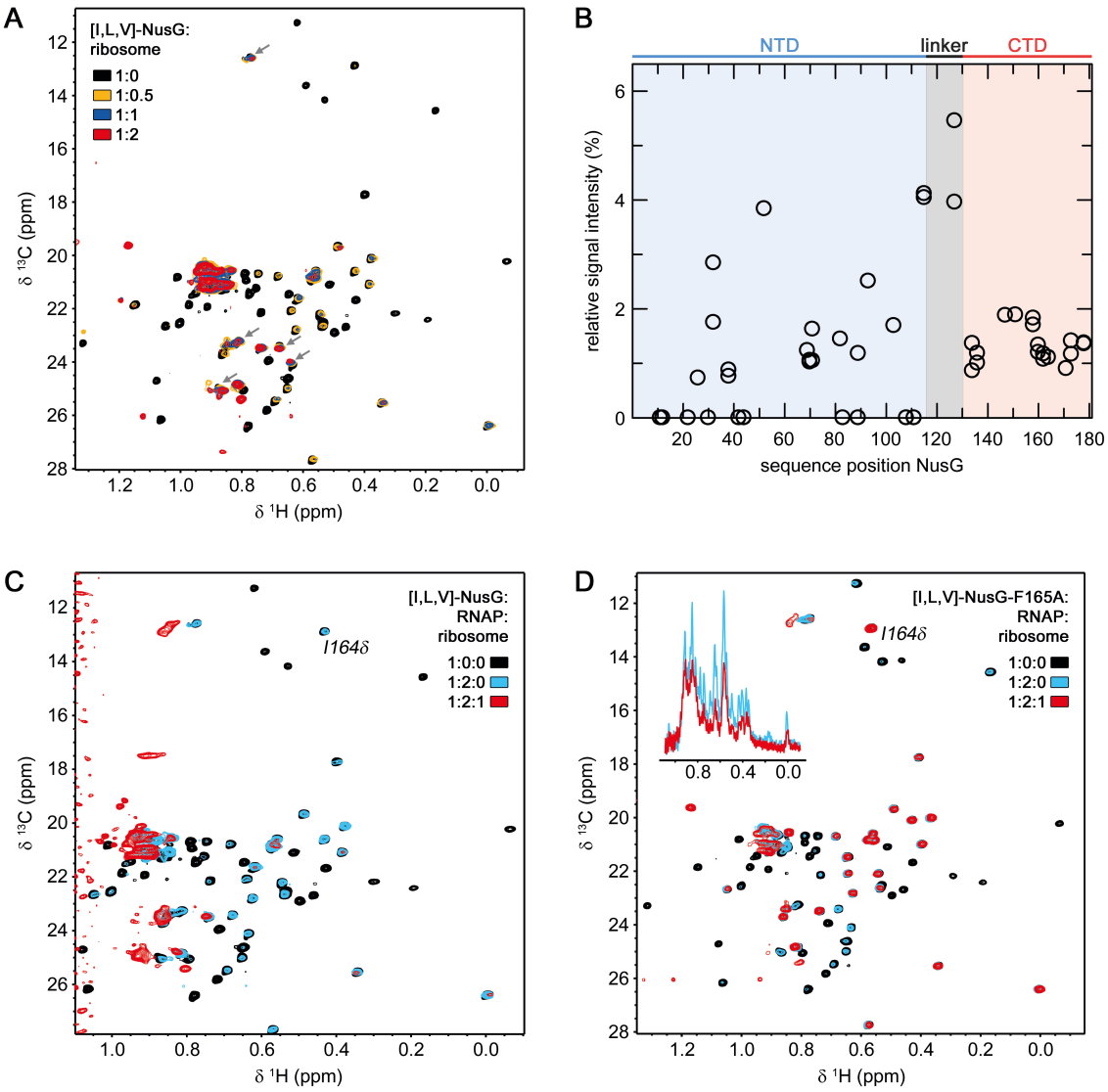

Figure 3: RNAP-bound NusG interacts with the 70 S ribosome. (A,B) NusG interacts with 70S ribosome via its CTD. **(A)** 2D [^{1}H, ^{13}C]-methyl-TROSY spectra of free [ILV]-NusG (11 µM, black) and [ILV]-NusG in the presence of 70S ribosome (molar ratio [ILV]-NusG:ribosome = 1:0.5 (6.6 µM [ILV]-NusG, orange); = 1:1 (7.5 µM [ILV]-NusG, blue); =1:2 (4 µM [ILV]-NusG, red). Arrows indicate [ILV]-NusG-NTD signals that are well visible in the [ILV]-NusG:ribosome complex. **(B)** Quantitative analysis of [ILV]-NusG methyl group signal intensities in the presence of 0.5 equivalents of 70S ribosome. Relative signal intensities are plotted versus the sequence position of NusG.

769 The domain organization of NusG is indicated above the diagram. **(C)** 2D [^{1}H, ^{13}C]-
770 methyl-TROSY spectra of [ILV]-NusG (11 μM, black), [ILV]-NusG in the presence of
771 RNAP (molar ratio 1:2, 6 μM [ILV]-NusG, blue), and [ILV]-NusG in the presence of
772 RNAP and 70S ribosome (molar ratio 1:2:1, 6 μM [ILV]-NusG, red). **(D)** 2D [^{1}H, ^{13}C]-
773 methyl-TROSY spectra of [ILV]-NusG^{F165A} (20 μM, black), [ILV]-NusG^{F165A} in the
774 presence of RNAP (molar ratio 1:2, 6 μM [ILV]-NusG^{F165A}, blue), and [ILV]-NusG^{F165A}
775 in the presence of RNAP and 70S ribosome (molar ratio 1:2:1, 6 μM [ILV]-NusG^{F165A},
776 red). The inset shows the normalized 1D spectra of the corresponding titration step.
777

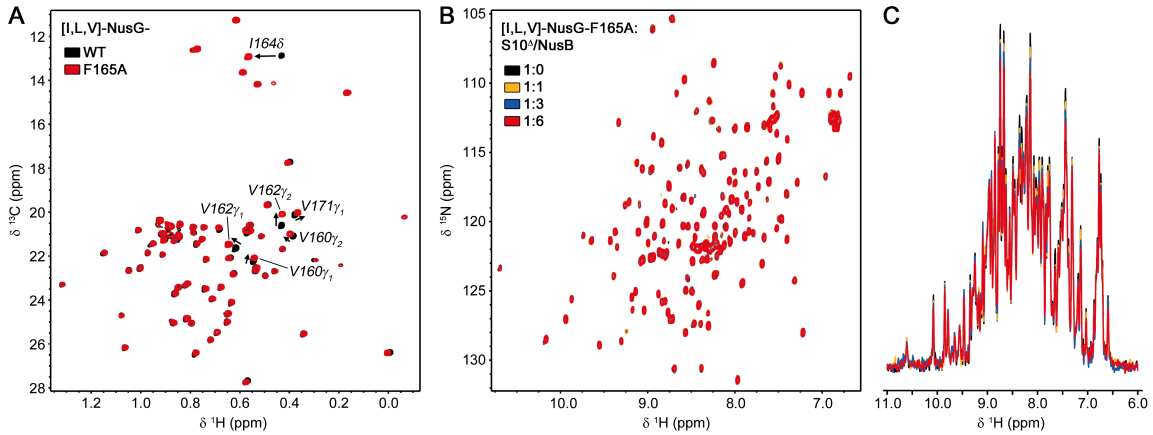

778

779 **Figure 3-figure supplement 1: NusG-F165A does not interact with S10^{A}/NusB. (A)**

780 2D [^{1}H, ^{13}C]-methyl-TROSY spectra of [ILV]-NusG (11 µM, black) and [ILV]-

781 NusG^{F165A} (20 µM, red). Arrows and labels indicate NusG-CTD methyl groups affected

782 in their resonance frequencies by the F165A amino acid substitution. **(B,C)** 2D **(B)** and

783 normalized 1D **(C)** [^{1}H, ^{15}N]-HSQC spectra of 20 µM [ILV]-NusG^{F165A} upon titration

784 with 432 µM S10^{A}/NusB (colors as indicated).

785

786

787

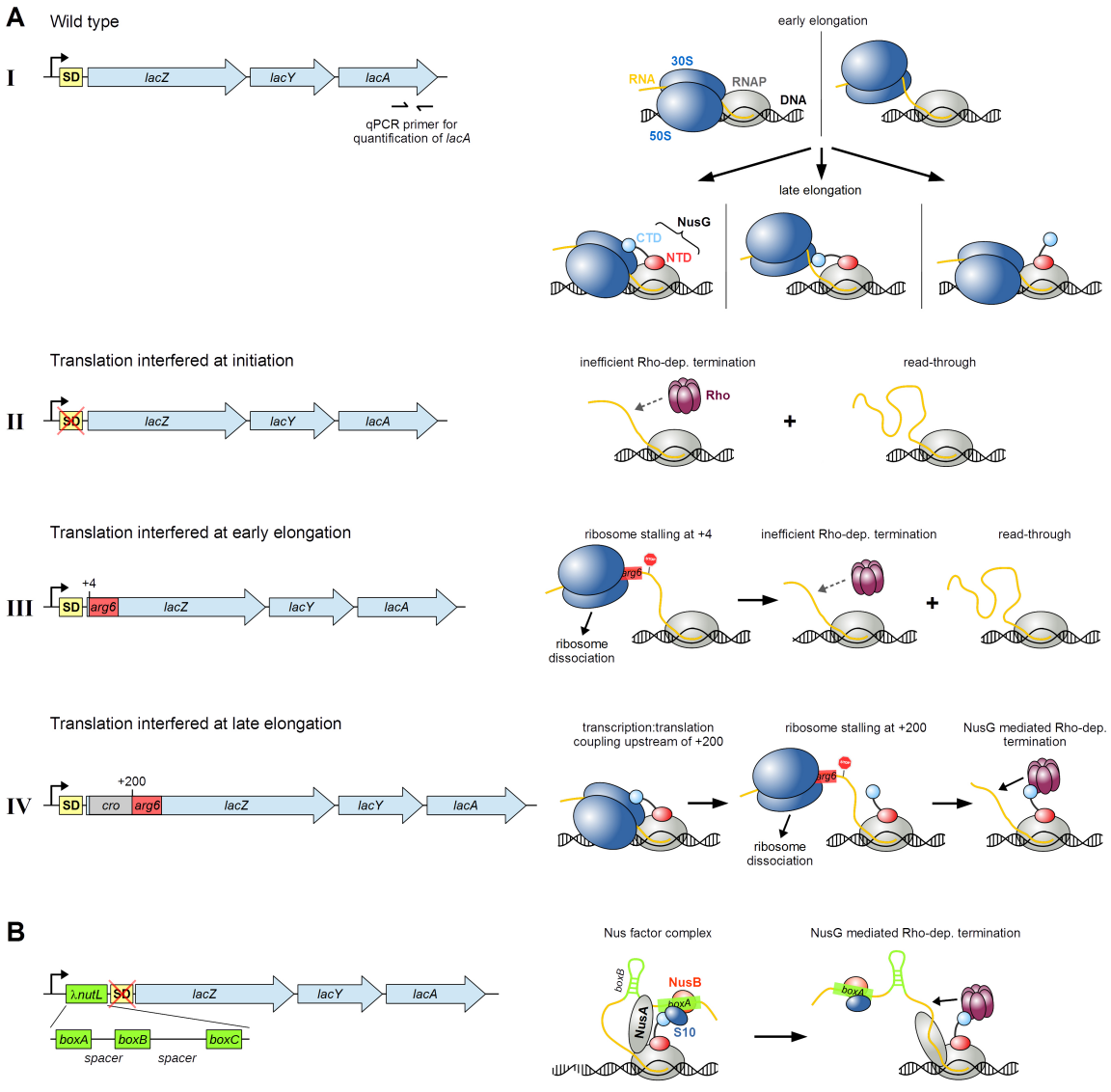

788

789 **Figure 4: Translation is required for NusG recruitment to the TEC. (A, B)** Left:

790 Organization of the *E. coli lac* operon in strains MDS42 (A-I; wild type *lacZ*), RSW1225

791 (A-II; mutant (inactive) *lacZ* SD sequence), RSW1245 (A-III; in-frame insertion of six

792 rare Arg codons (*arg6*) at position +4 of *lacZ*), RSW1276 (A-IV; in-frame insertion of

793 λ*cro* and six rare Arg codons at position +4 of *lacZ* (equivalent to *arg6* being at position

794 +200 of the gene)), and RSW1297 (B; λ*nutL* site upstream of mutant *lacZ* SD sequence).

795 SD sequences of *lacY* and *lacA* were omitted for clarity. qPCR primers specific to the 3'

796 end of *lacA* (position indicated in A-I) were used to measure mRNA levels and thereby

797 read-through of *lacA* (see Table 1). Right: Schemes of possible effects on
798 transcription:translation coupling and Rho-dependent termination within *lacZ*. A-I, top:
799 Ribosomes are recruited in the early elongation phase, leading to a directly coupled
800 RNAP:ribosome complex (left) or uncoupled transcription and translation (right). A-I,
801 bottom: NusG is recruited in late elongation, resulting in a NusG-coupled complex with
802 (left) or without direct RNAP:ribosome contacts (middle), or modifying the pre-existing
803 RNAP:ribosome complex without establishing an CTD:S10 interaction (right). A-II:
804 Failure of NusG recruitment results in inefficient Rho-dependent termination and high
805 *lacA* read-through. A-III: *arg6* stops the translating ribosome at position +4, whereas
806 transcription elongation proceeds (left), resulting in ribosome dissociation and no NusG
807 recruitment. Transcription proceeds and is only inefficiently terminated by Rho (right).
808 A-IV: NusG couples transcription and translation (left) until *arg6* stops the ribosome at
809 position +200 (middle), allowing efficient, NusG-stimulated Rho-dependent termination
810 (right). B: λ*nutL* recruits NusA, NusG and the S10/NusB dimer, creating a Nus complex
811 (left). NusG can thus support Rho-dependent termination.
812
813

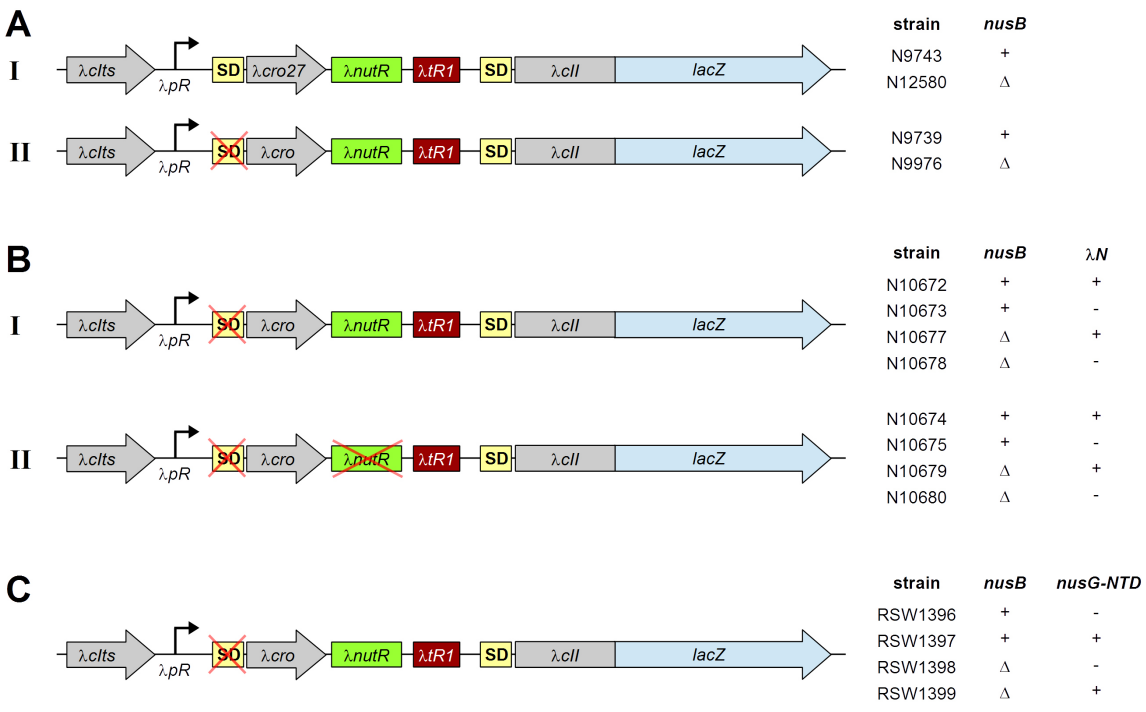

Figure 5: NusG can be recruited *via* a Nus complex. Genetic constructs used to monitor NusG mediated Rho-dependent termination are shown with the corresponding strains and their properties indicated on the right side. Transcription is started from the λ*pR* promoter, followed by WT-λ*cro* or λ*cro* carrying a missense mutation at codon 27 (λ*cro27*), a WT or mutant λ*nutR* site (B), the Rho-dependent terminator λ*tR1* and a λ*cII::lacZ* transcriptional fusion with corresponding SD site. All strains encode a temperature sensitive λcI construct (λ*cIts*) to allow temperature-controlled induction of gene expression from the λ*pR* promoter. λN^{+} strains listed in (B) further encode the λN protein; NusG-NTD for strains listed in (C) was supplied from plasmid pRM442. See also tables 2A-C.

826 **Tables**

827

828 **Table 1. NusG couples late after transcription initiation.** β-galactosidase was induced
829 for 20 min from the *lac* operon with1mM IPTG. Where indicated, Rho-dependent
830 termination was inhibited by adding 100μg/ml BCM 1 minute prior to induction. Read-
831 through was calculated from the fold-increase of *lacA RNA* compared to *ompA* RNA in
832 the presence or absence of BCM. RNA levels were measured using qRT-PCR and the
833 fold- increase calculated using the $\Delta\Delta C_t$ method (Livak and Schmittgen, 2001).
834 RSW1225 carries two G to A mutations in the *lacZ* ribosome-binding site. RSW1245
835 carries an insertion of six rare arginine codons (atg-acc-atg-AGG-AGA-CGA-AGG-
836 AGA-CGA) at the amino terminus of *lacZ*. RSW1276 contains six rare arginine codons
837 200nt distal to the start of translation. RSW1297 carries an insertion of λ*nutL*
838 immediately 5' to the mutated ribosome binding site.

strain	*lacZ*	*nutL*	BCM$^-$	BCM$^+$	RT (%)
MDS42	wt	-	.25	.26	99
RSW1225	SD$^-$	-	.12	.56	21
RSW1245	arg(6) - early	-	.13	.49	29
RSW1276	arg(6) - late	-	<.01	.12	<1
RSW1297	SD$^-$	+	.01	.59	1

839

Table 2. NusG recruitment depends on translation. (A) NusG coupling at *nutR* requires NusB. Expression of β-galactosidase was induced from a chromosomal *cII*::lacZ transcriptional fusion (λ*cIts-pR-cro-nutR-tR1-cII::lacZ*) by incubating at 42^0 C for 30 min. N9743 and N12580 carry a missense mutation at *cro* codon 27, N9739 and 9976 have a G to C mutation in the *cro* Shine Dalgarno sequence (*SD*-), N12580 and N9976 are deleted for *nusB*. Where indicated, bicyclomycin (BCM) was added to 100μg/ml prior to induction of β-galactosidase. Read-through (RT) was calculated from the ratio of β-galactosidase activity in the presence or absence of BCM. **(B)** BoxA mutations block NusG coupling at *nutR*. Expression of β-galactosidase was induced from a chromosomal *cII*::lacZ transcriptional fusion (λ*cIts-pR-cro* (*SD*$^-$) *-nutR-tR1-cII::lacZ*) by incubating at 42^0 C for 30 min. Strains N10672, N10674, N10677 and N10679 express the λN transcription termination inhibitor. *boxA69* and Δ*nusB* strain numbers are indicated in Table 3. Read-through (RT) was calculated from the ratio of β-galactosidase activity in the presence or absence of λN. **(C)** NusG-NTD uncouples. Expression of β-galactosidase was induced from a chromosomal *cII*::lacZ transcriptional fusion (λ*cIts-pR-cro(*SD$^-$*)-nutR-tR1-cII::lacZ*) by incubating at 42^0 C for 30 min. The NusG-NTD was induced from the plasmid pRM442 *tac* promoter with 1mM IPTG for 10 min prior to induction of β−galactosidase in strains RSW1397 and RSW 1399. Strains RSW1396 and RSW1398 carried an empty vector (p*trc99A*) and were exposed to IPTG as above. Where indicated bicyclomycin (BCM) was added to 100μg/ml prior to induction of β-galactosidase. Read-through (RT) was calculated from the ratio of β-galactosidase activity in the presence or absence of BCM.

862

A	strain	*cro*	*nusB*	BCM$^-$	BCM$^+$	RT (%)
	9743	*ms27*	+	530	680	78
	12580	*ms27*	D	890	1150	78
	9739	SD-	+	141	613	**23**
	9976	SD-	D	1191	1290	92

863

B	strain	*boxA*	*nusB*	λN$^-$	λN$^+$	RT (%)
	10673, 10672	+	+	126	946	**13**
	10675, 10674	*69*	+	1212	2211	55
	10678, 10677	+	D	2874	2616	100
	10680, 10679	*69*	D	1896	2416	78

864

C	strain	*nusG-NTD*	*nusB*	BCM$^-$	BCM$^+$	RT (%)
	RSW1396	-	+	247	862	**29**
	RSW1397	+	+	944	1013	93

	RSW1398	–	Δ	2013	2314	93
	RSW1399	+	Δ	2360	2760	86

865

866

867